ANALYSIS OF EXTERIOR ORIENTATION PARAMETERS ON MONOPLOTTING PROCEDURE FOR AVOIDING OBSTACLES IN UAV REAL-TIME ROUTING

D. P. Simões [1], H. C. de Oliveira [2], R. L. dos Santos [1]

[1] School of Civil Engineering, Architecture and Urban Design of University of Campinas - Unicamp, Campinas, Brazil - (d263621, r228749)@dac.unicamp.br

[2] Department of Surveying Engineering, Penn State University - Wilkes-Barre, Pennsylvania, USA - hmo5157@psu.edu

KEYWORDS: Monoplotting, Unmanned Aerial Vehicle, Online Path Plan, Propagation of Variance and Covariance, Mapping.

ABSTRACT:

Unmanned Aerial Vehicles (UAVs) are adopted in different applications, such as mapping, logistics, and surveillance. For some applications, it is important to identify people or objects to be tracked in the image and define their coordinates in the object space. It can be done by using a photogrammetric process called Monoplotting. Moreover, by applying the Propagation of Variance and Covariance, the standard deviation from planimetric coordinates can be defined as an Exterior Orientation Parameter (EOP) function. This work evaluates the planimetric accuracy achieved using points defined in UAV images and the impact of EOPs precision. Two UAV images, the Digitals Surface Model (DSM) from the corresponding areas, the EOPs (X0, Y0, Z0, ω, φ, κ), and the platform/sensors characteristics were used for the experiments. Results showed that planimetric precision is low when using UAVs with a low-cost positioning system, especially if the points of interest in the image are far from the nadir. For UAVs with a high-precision positioning system, Inertial Measurement Unit (IMU) system is the one with a higher influence on the accuracy of planimetric coordinates, especially for oblique photographs (essential for UAV routing when avoiding obstacles). The impact of the IMU system precision increases in oblique photographs, this alerts to attention for UAV flight real-time routing guided by obstacles mapping using images.

1. INTRODUCTION

Advanced Technologies in Unmanned Aerial Vehicles (UAVs), also known as drones, have been used in a greater number of applications. Some examples include mapping, logistics, security, surveillance, traffic management, agriculture, aeronautics, and several military applications. However, the increasing use of UAVs concerns airspace management and people safety (it is presented in more detail in Section 2.1).

Tan et al. (2019) highlight path planning, among other elements, as an alternative, to ensure the safety and efficiency of the Unmanned Aerial System (UAS) Traffic Management (UTM). Researchers have been studying safe path planning for UAVs for many years. As an example, the recent study developed by Simões et al. (2022a) addresses UAV path planning by using high-resolution photogrammetric products. The authors also highlighted the concern about following the rules of access to airspace, creating offline routes that bypass the no-fly zones.

The no-fly zones can be characterized as areas where flying is prohibited due to proximity to buildings, airports, or military areas, for example. Thus, it is possible to map these places in advance and avoid them on a safe flight with a UAV. However, it is difficult to map or even model the location of people on the ground during flight time. Identifying people in real-time during a UAV flight is crucial to keep the operation safe in some applications. This is especially important for online path planning. The identification and tracking of people and objects are also important for the surveillance of smart cities (Surinta and Khruahong, 2019), as shown by Del Rosario et al. (2021). In these surveillance applications, wired drones are widely used

(Walendziuk et al., 2020), to obtain vertical images from where the objects of interest are identified.

In these applications, it is important to identify people or objects in the image and define the corresponding element coordinates in the object space (X, Y, and Z). It can be done by using Artificial Intelligence, especially Deep Learning techniques (Srivastava et al., 2021; Lu et al., 2023).

The determination of obstacles (or kinematic no-flying zones) coordinates on the ground can be carried out by the photogrammetric process known as Monoplotting, which uses a UAV image and the Digital Terrain Model (DTM) from the study area - more details in Section 2.2. In this process, it is necessary to know the Exterior Orientation Parameters (EOPs) of the image: perspective center coordinates and camera attitude at the moment of the image acquisition. Therefore, the standard deviation of the planimetric coordinates can be determined by applying the Propagation of Variance and Covariance (Ghilani, 2017) - described in Section 2.3 - as a function of the EOPs.

This research evaluates the planimetric precision achieved for points defined in UAV images and evaluates the influence of EOPs for the standard deviation of the objects' planimetric coordinates on the ground and their precision. This is crucial to define which UAV should be adopted for a specific application.

This article is structured as follows: Section 2 presents a Literature Review including some main concepts used in this work. Section 3 highlights the materials and the proposed method. Section 4 describes the experiments carried out to validate the proposed methodology. Finally, Section 5 presents the authors' conclusion for this work.

2. LITERATURE REVIEW

2.1 Airspace security

The growing use of UAVs in airspace can be seen worldwide. In April 2023, there were 878,721 registered drones just in the United States of America (FAA, 2023). Consequently, airspace safety becomes a concern. Rubio-Hervas et al. (2018) highlighted the need for UTM to minimize the risks in UAV operations.

Therefore, it is necessary to follow specific rules for managing UAV traffic, as highlighted by Stöcker et al. (2017). All over the world, there are regulations on airspace access and control, seeking to minimize the risks of UAVs operations, especially for people interaction. Although there is no single regulation around the world (Stöcker et al., 2017), there is a concern related to people's safety. In some countries including Brazil (Brasil, 2020), European Union (European Union, 2019), the United Kingdom (CAA, 2020), and Australia (CASA, 2020), for example, regulation for airspace access requires a minimum distance between the UAV position projected on the ground and people.

Thus, an important element for the UTM is path planning which is responsible for ensuring the distance between people and the UAV. There are different path-planning methods for UAVs. They can be classified according to the time domain (online or offline), the environment model (two-dimensional or three-dimensional), and aircraft characteristics (fixed wing, multirotor and hybrid) (Simões et al., 2022b).

For online path planning, the aircraft identifies risks in the environment and must react, updating the route in real-time. In offline routing, the UAV executes a path planned based on pre-existing and fixed information, sometimes relying only on obstacle avoidance (near the aircraft). The route is two-dimensional when the flight height remains constant along the entire path. If the flight height changes during the path as a function of the terrain conditions, the route is considered three-dimensional (Zhao et al., 2018).

2.2 Monoplotting

Monoplotting is a photogrammetric procedure that allows obtaining the three-dimensional coordinates (X, Y, Z) of a point in the object space from measurements in image space, using only one image. For this process, a Digital Terrain Model (DTM) and a raw image in which Orientation Parameters are known, are required (Fluehler et al., 2005).

Determining the coordinates from a DTM and a single image is performed by back projecting the coordinates in a given plane. In this case, the coordinates are projected at a fixed elevation (Z coordinate) and the solution for X and Y is obtained directly by using the Inverse Collinearity Equations (Mikhail et al., 2001).

Once the initial coordinates of a point (X_i, Y_i) are determined from the maximum DTM elevation (Z_i), a new elevation value (Z_{i+1}) is interpolated into the DTM. With this current elevation value, a new position is calculated (X_{i+1}, Y_{i+1}). This process is iterative and it ends when changes in coordinate values X and Y are within a threshold (Fluehler et al., 2005). Authors, such as Mikhail et al. (2001), also name this process as single-ray back-projection.

2.3 Propagation of variance and covariance

All observations present some errors, and they are all propagated to indirect measures (Ghilani, 2017). The propagation of variance and covariance is also known as the propagation of errors (Mikhail and Ackermann, 1976), and is common to use it in Geodetic Sciences, such as in Photogrammetry, to evaluate measures obtained from certain parameters.

Considering a function Z involving n variables ($x_1, x_2, x_3, ..., x_n$), the standard deviation of Z is given by Equation 1 (Ghilani, 2017).

$$\sigma_Z = \sqrt{\left(\frac{\partial Z}{\partial x_1}\, \sigma_{x_1}\right)^2 + \left(\frac{\partial Z}{\partial x_2}\, \sigma_{x_2}\right)^2 + \cdots + \left(\frac{\partial Z}{\partial x_n}\, \sigma_{x_n}\right)^2} \quad (1)$$

$$\Sigma_{ZZ} = A * \Sigma * A^T \quad (2)$$

Equation 1 can be considered when the variables ($x_1, x_2, x_3, ..., x_n$) are independent. In this case, the covariance (σ_{xixj}) between two variables is zero. The greater the interdependence between two variables, the greater the covariance between them (Ghilani, 2017).

Equation 2 presents the variance-covariance matrix for function Z. A is the design matrix (also known as Jacobian or partial derivatives matrix), and Σ is the variance-covariance matrix for variables x_i. Considering linear equations and independent variables, the general law of propagation of variances can be updated for the Special Law of Propagation of Variances (SLOPOV) (Ghilani, 2017).

Equation 1 represents how the errors of statistically independent observations propagate in a function. The individual contribution of the observation error of each independent variable is presented in the individual terms of this equation. Therefore, one way to analyze (and mitigate) the overall error of a function is to analyze the error of individual terms. This allows the identification of the observations that contribute the most to the function's overall error (Ghilani, 2017) – in our case, the position of no-fly zones.

3. MATERIAL AND METHOD

This work was based on images obtained with a UAV. Moreover, it includes the Interior Orientation (IOP) and Exterior Orientation (EOP) parameters of the images, and the Digital Surface Model (DSM) of the study area – a point cloud. Both EOP and DSM were obtained from photogrammetric process of UAV imagery.

Through these data, the Monoplotting photogrammetric process (Section 3.1) and the propagation of variance and covariance (Section 3.2) were implemented to determine the standard deviation of planimetric coordinates in object space.

3.1 Monoplotting

First, the coordinates in the image system (column, row) were defined. By knowing the IOPs and camera characteristics, the coordinates were converted into the photogrammetric coordinate system (x, y, -f) – coordinate refinement and conversion.

From an arbitrary Z coordinate, the planimetric coordinates in the object space (X and Y) were obtained by using the Inverse Collinearity Equations. Then, the Z coordinate in the DTM corresponding to the calculated X and Y coordinates were calculated by an interpolation process. The DTM was obtained from a DSM filtering process using the LAStools library (Isenburg, 2021).

The difference between the Z coordinate calculated and the one obtained from the DTM interpolation is defined. Iterations were performed until a stopping threshold could be reached (The used threshold was 0.1 m). Finally, from the final Z coordinate determined after the iterative process, the corresponding X and Y coordinates were calculated by using the Inverse Collinearity Equations.

3.2 Propagation of variance and covariance

Considering the influence of the EOPs (X0, Y0, Z0, ω, φ, and κ) on the X and Y coordinates of the points in the object space, the propagation of variance and covariance was carried out. As input data, values of planimetric, altimetric, and angular precision were defined from UAV's positioning system (σ_{X0}, σ_{Y0}, and σ_{Z0} were defined from the Global Navigation Satellite Systems - GNSS, and σ_{ω}, σ_{φ}, and σ_{κ} - were established from Inertial Measurement Units system - IMU).

Therefore, the standard deviations of X (Equation 3) and Y (Equation 4) coordinates were defined from the partial derivatives of the Inverse Collinearity Equations as a function of the EOPs, together with the standard deviation of planimetric ($\sigma_{X0} = \sigma_{Y0}$), altimetric ($\sigma_{Z0}$), and angular ($\sigma_{\omega} = \sigma_{\varphi} = \sigma_{\kappa}$) variables.

$$\sigma_X = \sqrt{\begin{aligned} &\left(\frac{\partial X}{\partial X0}\right)^2 * \sigma_{X0}^2 + \left(\frac{\partial X}{\partial Y0}\right)^2 * \sigma_{Y0}^2 + \left(\frac{\partial X}{\partial Z0}\right)^2 * \sigma_{Z0}^2 + \\ &+ \left(\frac{\partial X}{\partial \omega}\right)^2 * \sigma_{\omega}^2 + \left(\frac{\partial X}{\partial \varphi}\right)^2 * \sigma_{\varphi}^2 + \left(\frac{\partial X}{\partial \kappa}\right)^2 * \sigma_{\kappa}^2 \end{aligned}}$$

(3)

$$\sigma_Y = \sqrt{\begin{aligned} &\left(\frac{\partial Y}{\partial X0}\right)^2 * \sigma_{X0}^2 + \left(\frac{\partial Y}{\partial Y0}\right)^2 * \sigma_{Y0}^2 + \left(\frac{\partial Y}{\partial Z0}\right)^2 * \sigma_{Z0}^2 + \\ &+ \left(\frac{\partial Y}{\partial \omega}\right)^2 * \sigma_{\omega}^2 + \left(\frac{\partial Y}{\partial \varphi}\right)^2 * \sigma_{\varphi}^2 + \left(\frac{\partial Y}{\partial \kappa}\right)^2 * \sigma_{\kappa}^2 \end{aligned}}$$

(4)

4. EXPERIMENTS AND DISCUSSION

In this section, experiments were carried out to analyze the planimetric bias and precision of points obtained from the Monoplotting (Sections 4.1 and 4.2), and how the EOPs influence the precision (Section 4.3). As input data, it was adopted two UAV images, the Digital Surface Model from the corresponding areas, the images' EOP, and the camera IOP.

4.1 Planimetric bias analysis

To evaluate the planimetric bias, it was used two images and eight points were defined in each image (Figures 1 and 2). Table 1 presents the EOPs of Images 1 and 2, obtained with flight heights of approximately 20 m and 40 m, respectively.

The coordinates in the digital system (column, row) of the points were determined, and the three-dimensional corresponding 3D coordinates (X, Y, Z) were calculated.

Tables 2 and 3 present the difference (bias) between the coordinates calculated by Monoplotting and the coordinates of the points defined using photogrammetric products (orthophoto mosaic and DSM) for Images 1 and 2, respectively.

	Image 1	Image 2
X0 (m)	288,671.911150	362,452.894182
Y0 (m)	7,475,369.632991	7,532,194.419143
Z0 (m)	660.463484	925.654137
ω (°)	0.276545	-21.414538
φ (°)	-0.585221	-12.586993
κ (°)	176.963692	-152.342339

Table 1. Exterior Orientation Parameters: Images 1 and 2.

Figure 1. Image 1: location of the points adopted in the experiments.

Point	ΔX (m)	ΔY (m)	ΔZ (m)	Planimetric Error
1	0.110	-0.009	0.016	0.110
2	0.098	0.056	0.049	0.113
3	0.098	0.087	0.018	0.131
4	0.209	0.048	-0.006	0.214
5	-0.041	-0.065	0.077	0.064
6	0.192	0.055	0.010	0.200
7	-0.095	0.003	-0.003	0.095
8	-0.006	0.194	-0.019	0.194
Mean error		**0.003**		**0.142**

Table 2. Difference between calculated and measured coordinates – Image 1.

Figure 2. Image 2: location of the points adopted in the experiments.

Point	ΔX (m)	ΔY (m)	ΔZ (m)	Planimetric Error
1	-0.472	0.577	-0.015	0.746
2	-0.095	0.267	-0.038	0.283
3	-0.122	-0.017	0.005	0.123
4	0.102	-0.408	-0.013	0.420
5	-1.168	0.825	0.186	1.430
6	-0.002	-1.965	-0.152	1.965
7	1.264	-0.854	0.222	1.525
8	-0.227	1.367	0.006	1.385
Mean error			**0.025**	**0.985**

Table 3. Difference between calculated and measured coordinates – Image 2.

For Image 1 (Figure 1 and Table 2), the average altimetric error is insignificant for this application. The average planimetric error is 14.2 cm. It is an error that cannot be ignored for some applications, such as precision mapping. However, for many applications, such as path planning for UAVs, this error is irrelevant, considering for example the dimensions of a UAV and the regulations limits (buffer from the UAV position projected on the ground).

For Image 2 (Figure 2 and Table 3), the average altimetric error is 2.5 cm which is also insignificant for path planning application. However, the average planimetric error is higher - approximately 1 m. For points 5, 6, 7, and 8, the planimetric error is greater than 1 m. These points are the farthest in distance from the image center. The systematic errors of images - principal point displacement, symmetrical radial distortion, and decentering distortion - were not corrected, which can influence the high planimetric errors. Furthermore, Image 2 was obtained with a higher flight height, if compared to Image 1. This also may add to the errors of the points' coordinates located in the image borders.

4.2 Planimetric precision analysis

To evaluate the planimetric precision of the coordinates obtained from the Monoplotting procedure, three experiments were performed for each image through the SLOPOV. For each experiment, it was simulated the use of a different UAV, considering the values of σ_{X0}, σ_{Y0}, and σ_{Z0} defined by GNSS system precision, and the values of σ_{ω}, σ_{φ}, σ_{κ} estimated from the precision of the IMU system. In this way, we can evaluate how the precisions of the GNSS and IMU on board the UAV interfere on the precision of the X and Y coordinates of the projected points on the ground.

The first experiment considers the positioning system of a Phantom 4 Pro drone. For the second experiment, a Matrice UAV with GNSS RTK positioning was considered (DJI, 2023a) – for the angular accuracy, the accuracy of the Zenmuse L1 sensor IMU system was considered (DJI, 2023b). For the third experiment, the standard deviation values were defined considering a low-cost UAV. Table 4 presents the values of planimetric (σ_{X0} and σ_{Y0}), altimetric (σ_{Z0}), and angular (φ_{ω}, σ_{φ}, σ_{κ}) standard deviations for the experiments – 1 and 3 consider a low precision system on board, and 2 corresponds higher precision system.

Experiment	System precisions considered		
	$\sigma_{X0} = \sigma_{Y0}$ (m)	σ_{Z0} (m)	$\sigma_{\omega} = \sigma_{\varphi} = \sigma_{\kappa}$ (°)
1	5	10	2
2	0.01	0.015	0.3
3	10	15	2

Table 4. Planimetric, altimetric, and angular standard deviations used in the experiments.

Figures 3 and 4 present the planimetric standard deviation for eight points tested for Images 1 and 2, respectively. Planimetric precision is low for all points in experiments 1 and 3. This result is expected considering the low initial planialtimetric precision (σ_{X0}, σ_{Y0}, and σ_{Z0}). In the opposite way, considering the high precision of the positioning system used in the second experiment, the planimetric precision of the points tested in Experiment 2 is higher.

In Image 1 (Figure 3), points from 4 to 8 presents the largest standard deviation. These points are located further away from the nadir point of the image, which explains the worse precision in the final X and Y coordinates in this image. It can be considered a vertical image according to EOPs (Table 1) - ω and φ are less than 3°.
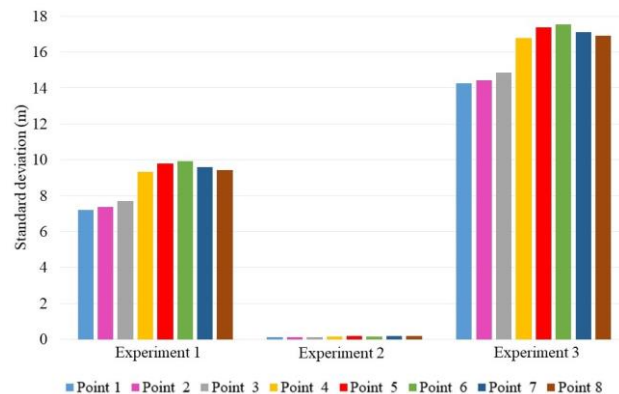
Figure 3. Standard deviation for the three experiments using Image 1.

For Image 2 (Figure 4), as it is an oblique aerial photograph (ω and φ are greater than 3°), it is observed that the standard deviation increases according to the distance between the UAV and the ground point. For example, points 6 and 7 are the further of the UAV position at the moment of image acquisition.
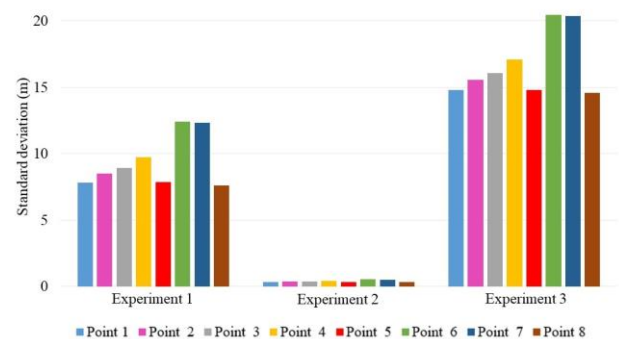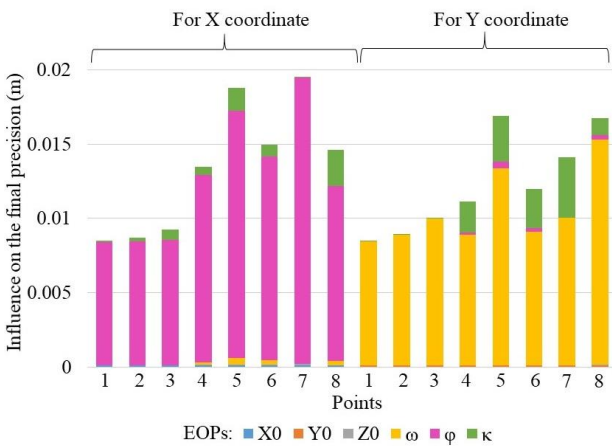

Figure 4. Standard deviation for the three experiments using Image 2.

## 4.3 The individual impact of EOPs on planimetric accuracy

In this section, it is presented the influence of each EOP on the final precision of the X and Y coordinate (Figures 5 to 10).
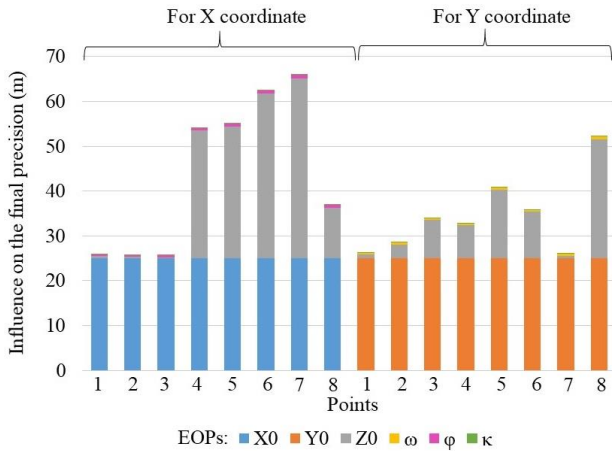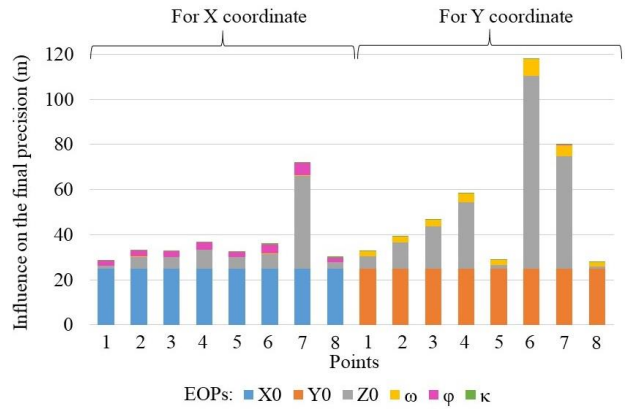

Figure 5. Influence of EOPs on the final precision of the X and Y coordinate for the Experiment 1 ($\sigma_{X0} = \sigma_{Y0} = 5$ m; $\sigma_{Z0} = 10$ m; $\sigma_\omega = \sigma_\varphi = \sigma_\kappa = 2°$) – Image 1.
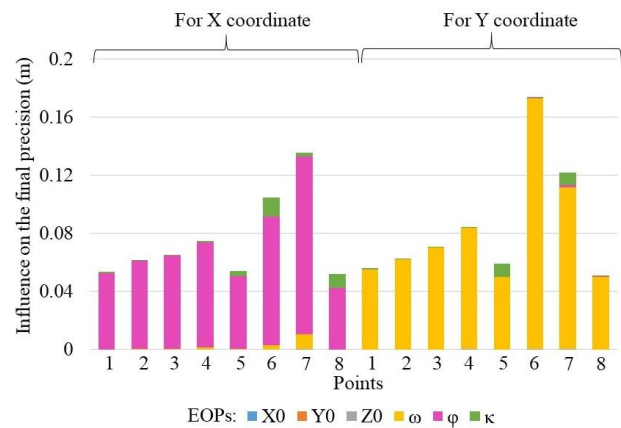

Figure 6. Influence of EOPs on the final precision of the X and Y coordinate for the Experiment 2 ($\sigma_{X0} = \sigma_{Y0} = 0.01$ m; $\sigma_{Z0} = 0.015$ m; $\sigma_\omega = \sigma_\varphi = \sigma_\kappa = 0.3°$) – Image 1.
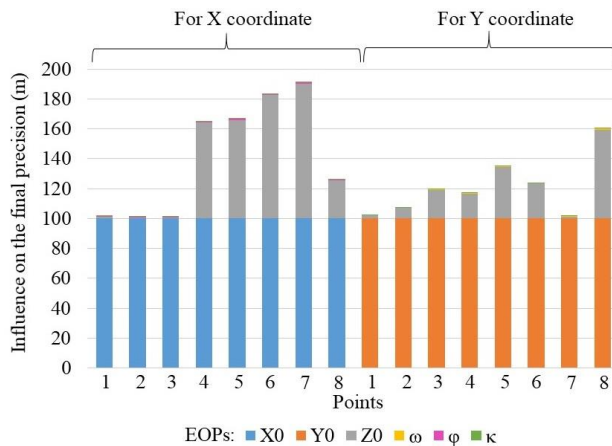
Figure 7. Influence of EOPs on the final precision of the X and Y coordinate for the Experiment 3 ($\sigma_{X0} = \sigma_{Y0} = 10$ m; $\sigma_{Z0} = 15$ m; $\sigma_\omega = \sigma_\varphi = \sigma_\kappa = 2°$) – Image 1.
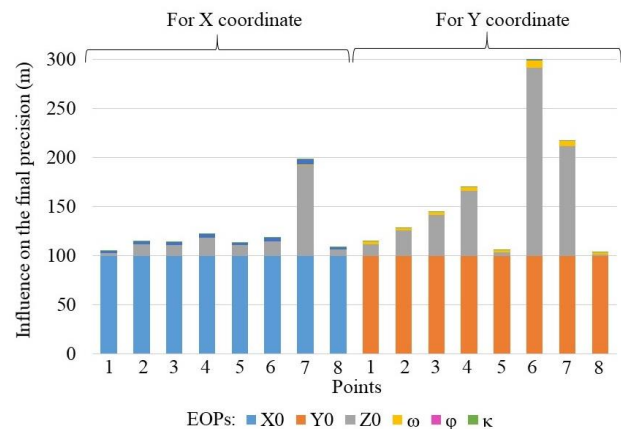

Figure 8. Influence of EOPs on the final precision of the X and Y coordinate for the Experiment 1 ($\sigma_{X0} = \sigma_{Y0} = 5$ m; $\sigma_{Z0} = 10$ m; $\sigma_\omega = \sigma_\varphi = \sigma_\kappa = 2°$) – Image 2.

Figure 9. Influence of EOPs on the final precision of the X and Y coordinate for the Experiment 2 ($\sigma_{X0} = \sigma_{Y0} = 0.01$ m; $\sigma_{Z0} = 0.015$ m; $\sigma_\omega = \sigma_\varphi = \sigma_\kappa = 0.3°$) – Image 2.

Figure 10. Influence of EOPs on the final precision of the X and Y coordinate for the Experiment 3 ($\sigma_{X0} = \sigma_{Y0} = 10$ m; $\sigma_{Z0} = 15$ m; $\sigma_\omega = \sigma_\varphi = \sigma_\kappa = 2°$) – Image 2.

The X0, Y0, and Z0 values have a significant impact on the final precision of the X and Y coordinates in experiments 1 and 3. These values represent how the GNSS system of the UAV affects the accuracy of the projected coordinates. Table 5 reveals that even with a high initial standard deviation from the IMU system, it has minimal influence on the final precision of the X and Y coordinates when the UAV's positional precision is low. This holds true for both Images 1 and 2 in experiments 1 and 3. However, in the case of experiment 2, where the GNSS

system has higher precision, it is the IMU system that primarily affects the precision of the planimetric coordinates, as indicated in Table 5.

	Experiment	GNSS (%)	IMU (%)
Image 1	1	98.51	1.49
	2	1.05	98.95
	3	99.57	0.43
Image 2	1	91.96	8.04
	2	0.18	99.82
	3	97.54	2.46

Table 5. Mean influence from UAV's GNSS and IMU systems the precision of the projected coordinates.

In experiments 1 and 3, the influence of Z0 is greater. For Image 1, especially the X coordinate precision of points 4 to 8 has a greatly influenced by Z0. These points are the ones with the highest discrepancies in X (Δx). For Y coordinate precision, the EOP Z0 also presents a greater influence on the points with the highest Y discrepancies (Δy). These points are the farthest points from the UAV during the image acquisition. For Image 2, the most influential of Z0 happens for the points further from the UAV. For both images, the weight of Z0 for X and Y precision is greater in Experiment 1, in which the value of the initial altimetric standard deviation value (σ_Z) is twice the planimetric standard deviation.

Figures 6 and 9 show that ω and φ are the EOPs that most influence the Y and X coordinates precision, respectively. For Images 1 and 2, ω and φ have a greater influence on the points farther from UAV. Furthermore, for the three experiments, Image 2 presents more influence of the IMU system if compared with experiments in Image 1: approximately 6.3 times greater. This can be explained by high values for the EOPs ω, and φ, of Image 2.

5. CONCLUSIONS

This paper presents that monoplotting procedure can be adopted in real-time applications - as UAV online routing. However, it is necessary that DSM been previously created. During the flight, it is important to have the UAV navigation system precision to be used as input for the monoplotting process. These results are low when using UAVs with low-cost positioning systems. For applications that require centimeter precision level, it is recommended to use UAVs with high-precision positioning systems, especially if the objects of interest in the image are far from the nadir point. This is important since planimetric accuracy is directly related to the distance between the UAV and the point on the ground.

For UAVs with a low-cost positioning system, the GNSS affects more than 90% of the planimetric precision of points on the ground. However, as important as the GNSS is the IMU system, once it is the system that influences the X and Y coordinate precision considering UAVs with high accuracy positioning system. This influence is about 6.3 times greater for oblique aerial photographs than for aerial vertical photographs/videos. Therefore, it is important to plan a UAV flight carefully, especially if the mission's goal requires the definition of the planimetric coordinates of points far away from the UAV position at the moment of image acquisition for kinematic no-fly zone determination.

For future works, the authors suggest this analysis with images acquired different flight heights from same area. This is an important element in the UAV flight planning and can interfere on the X and Y coordinates precision for oblique images, especially - that will be obtained during UAV online path planning.

REFERENCES

Brasil, 2020. ICA 100-40: Aeronaves Não Tripuladas e o Acesso ao Espaço Aéreo Brasileiro. *Departamento de Controle do Espaço Aéreo*. https://publicacoes.decea.mil.br/publicacao/ica-100-40 (6 February 2023).

CAA - Civil Aviation Authority, 2020. Unmanned Aircraft Systems: UAS Airspace Restrictions Guidance and Policy. CAP 722C. *Safety and Airspace Regulation Group*. https://publicapps.caa.co.uk/docs/33/CAP722C_Edition_2%20(p).pdf (6 February 2023).

CASA - Civil Aviation Safety Authority, 2020. CASR PART 101: Micro and excluded remotely piloted aircraft operations. https://www.casa.gov.au/sites/default/files/2021-08/part-101-micro-excluded-rpa-operations-plain-english-guide.pdf (6 February 2023).

Del Rosario, J. R. B., Bandala, A. A., Angeles, J. A. L., Cabebe, A. J. P., Co, J. J. D., Emmanuel, S. D., 2021. Development of a Multi-Object Detection and Human Tracking System from Cooperative Dual Cameras in an Unmanned Aerial Vehicle. *2021 IEEE 13th International Conference on Humanoid, Nanotechnology, Information Technology, Communication and Control, Environment, and Management (HNICEM)*. 1-4. IEEE. doi.org/ 10.1109/HNICEM54116.2021.9732035.

DJI, 2023a. *Matrice 300 RTK: Specifications*. https://www.dji.com/br/matrice-300/specs. (20 February 2023).

DJI, 2023b. *Zenmuse L1: Specifications*. https://www.dji.com/br/zenmuse-l1/specs. (20 February 2023).
European Union, 2019. COMMISSION IMPLEMENTING REGULATION (EU) 2019/947. https://eur-lex.europa.eu/legal-content/EN/TXT/PDF/?uri=CELEX:32019R0947&from=EN (6 February 2023).

FAA - Federal Aviation Administration, 2023. Drones by the Numbers. https://www.faa.gov/uas (29 April 2023).

Fluehler, M., Niederoest, J., Akca, D., 2005. Development of an educational software system for the digital mono-plotting. *International Archives of the Photogrammetry, Remote Sensing and Spatial Information Sciences*. 36(6). doi.org/10.3929/ethz-a-005126679.

Ghilani, C. D., 2017. *Adjustment computations: spatial data analysis.* John Wiley & Sons.

Isenburg, M., 2021. Lastools: Award-winning software for rapid lidar processing. Tech. Rep. lastools.github.io/ (30 March 2023).

Lu, W., Lan, C., Niu, C., Liu, W., Lyu, L., Shi, Q., Wang, S., 2023. A CNN-Transformer Hybrid Model Based on CSWin Transformer for UAV Image Object Detection. *IEEE Journal of Selected Topics in Applied Earth Observations and Remote Sensing*. 16. 1211-1231. doi.org/10.1109/JSTARS.2023.3234161.

Mikhail, E. M., Ackermann, F. E., 1976. *Observations and Least Squares:* With Contributions by F. Ackermann. IEP.

Mikhail, E. M., Bethel, J. S., McGlone, J. C., 2001. *Introduction to modern photogrammetry*. John Wiley & Sons.

Rubio-Hervas, J., Gupta, A., Ong, Y. S., 2018. Data-driven risk assessment and multicriteria optimization of UAV operations. *Aerospace Science and Technology*, 77, 510–523. doi.org/10.1016/j.ast.2018.04.001.

Simões, D. P., Oliveira H. C., Garcia, M. V. Y., 2022a. UAV 3-D Path Planning Based on High-Resolution DSM, DTM, and True Orthomosaic. *IEEE Geoscience and Remote Sensing Letters*. 19, 1-5. doi.org/10.1109/LGRS.2022.3219733.

Simões, D. P., Oliveira, H. C., Lima Júnior, O. F., Costa, D. C., 2022b. Métodos de Planejamento de Rotas para RPAs: uma Revisão da Literatura. *Revista Brasileira de Cartografia*. 74(2), 338–357. doi.org/10.14393/rbcv74n2-60138.

Srivastava, S., Narayan, S., Mittal, S., 2021. A survey of deep learning techniques for vehicle detection from UAV images. *Journal of Systems Architecture*, 117, 102152. doi.org/10.1016/j.sysarc.2021.102152.

Stöcker, C., Bennett, R., Nex, F., Gerke, M., Zevenbergen, J., 2017. Review of the Current State of UAV Regulations. *Remote sensing*. 9(5), 459. doi.org/10.3390/rs9050459.

Surinta, O., Khruahong, S., 2019. Tracking people and objects with an autonomous unmanned aerial vehicle using face and color detection. *2019 Joint International Conference on Digital Arts, Media and Technology with ECTI Northern Section Conference on Electrical, Electronics, Computer and Telecommunications Engineering (ECTI DAMT-NCON).* 206-210. IEEE. doi.org/ 10.1109/ECTI-NCON.2019.8692269.

Tan, Q., Wang, Z., Ong, Y., Low, K. H., 2019. Evolutionary Optimization-based Mission Planning for UAS Traffic Management (UTM). *Proc. 2019 Int. Conf. on Unmanned Aircraft Systems*, pp. 952-958. doi.org/10.1109/ICUAS.2019.8798078.

Walendziuk, W., Oldziej, D., Slowik, M., 2020. Power supply system analysis for tethered drones application. *2020 International Conference Mechatronic Systems and Materials (MSM).* 1-6. IEEE. doi.org/10.1109/MSM49833.2020.9202196.

Zhao, Y., Zheng, Z., Liu, Y., 2018. Survey on computational-intelligence-based UAV path planning. *Knowledge-Based Systems*. 158, 54–64. doi.org/10.1016/j.knosys.2018.05.033.